Received 30 May 2025; revised 24 June 2025; accepted 9 July 2025. Date of publication 11 July 2025; date of current version 22 August 2025.

Digital Object Identifier 10.1109/OJCOMS.2025.3588440

IRS-Assisted Wireless Sensor Networks With Hybrid TDMA-NOMA

HAITHAM AL-OBIEDOLLAH[1] (Member, IEEE), HAYTHEM BANY SALAMEH[2] (Senior Member, IEEE), AND KANAPATHIPPILLAI CUMANAN[3] (Senior Member, IEEE)

[1]Department of Electrical Engineering, Faculty of Engineering, The Hashemite University, Zarqa 13133, Jordan
[2]College of Engineering, Al Ain University, Al Ain, UAE
[3]School of Physics, Engineering and Technology, University of York, York, YO10 5DD, U.K.

CORRESPONDING AUTHOR: K. CUMANAN (e-mail: kanapathippillai.cumanan@york.ac.uk).

The work of Kanapathippillai Cumanan was supported by the U.K. Engineering and Physical Sciences Research Council (EPSRC) under Grant EP/X01309X/1.

ABSTRACT This paper investigates the energy harvesting (EH) and information decoding (ID) capabilities of wireless sensor networks (WSN) employing a hybrid time division multiple access (TDMA) and non-orthogonal multiple access (NOMA), i.e., the WSN with a hybrid TDMA-NOMA system. The system is assisted by a set of intelligent reflecting surface (IRS) units. In this configuration, the sensors are divided into a set of clusters, with each cluster consisting of two sensors. The available transmission time is equally divided into two phases: the downlink and uplink phases. In the downlink phase, the downlink time slot is dynamically split between the clusters into sub-time slots, where each sub-time slot is further divided into two slots, namely the wireless information transfer (WIT) and the wireless energy transfer (WET) slots. In the WIT slot, the sensors in the clusters use the received signal for ID, while the WET time slot is reserved for EH. However, in the uplink phase, the uplink time slot is also dynamically split into a set of slots, where each time slot is dedicated to assisting the uplink transmission from the sensors in each cluster to the base station (BS). To demonstrate the performance of such a system, we formulate a resource allocation framework that aims to minimize the total transmit power in the system while meeting a set of quality of service (QoS) requirements. Specifically, the total transmit power accounts for the downlink and uplink power, while the QoS requirements include a pre-defined minimum downlink data rate, minimum harvested energy for each sensor in the system, and minimum uplink data rate requirements. However, the joint nature of the optimization parameters in the downlink and uplink phases, namely power allocations in the downlink and uplink, time durations, and phase shift reflecting coefficients of the IRS units, as well as the non-convexity of the problem, introduces additional challenges in solving the formulated power minimization problem. To overcome these challenges, an iterative algorithm is proposed to solve the formulated optimization problem. To demonstrate the potential benefits of the proposed configuration, we present a set of simulations that evaluate its performance against two benchmarks: the IRS-free hybrid TDMA-NOMA system and the IRS-assisted hybrid TDMA-NOMA system with equal time allocations.

INDEX TERMS Intelligent reflecting surface (IRS), wireless sensor network (WSN), non-orthogonal multiple access (NOMA), Internet-of-Things (IoT), time division multiple access (TDMA), simultaneous wireless power and information transfer (SWIPT).

I. INTRODUCTION

WITH the advancement of Internet-of-Things (IoT) networks, communication systems are expected to support a wide range of emerging applications, such as monitoring human daily activities, sensing the surrounding environment, and facilitating industrial and medical tasks [1], [2]. In this context, wireless sensor networks (WSNs), which are categorized as promising IoT platforms,

have been widely deployed to perform a set of sensing services [3], [4]. Specifically, the WSN comprises a massive number of sensors that communicate their sensing information to a base station (BS) through both the uplink and the downlink [5]. However, the explosive growth of WSN has posed serious challenges, including supporting the massive number of sensors, handling their energy-constrained nature, and meeting the demanding quality-of-service (QoS) requirements of such networks [6].

Several research efforts have focused on meeting the massive connectivity requirements of WSNs. Specifically, it has been widely agreed that conventional orthogonal multiple access (OMA) techniques, i.e., time-division multiple access (TDMA) and orthogonal frequency division multiple access (OFDMA), will not be able to cope with the increased number of sensors. Accordingly, non-orthogonal multiple access (NOMA) has been recently identified as a potential multiple access technique for beyond fifth-generation (B5G) systems, including WSNs. In particular, unlike conventional OMA techniques, NOMA can serve more than one user in the same resource block (RB) through power-domain superposition coding (SC) at the transmitter end. At the receiver ends, users should be able to perform successive interference cancellation (SIC) to deal with the superimposed nature of the received signal. The SIC process introduces additional complexity to the detection process, restricting the deployment of NOMA in dense networks. Consequently, integrating NOMA with other OMA techniques can overcome this issue while introducing additional degrees of freedom, thereby supporting more users. Consequently, the combination of TDMA and NOMA, known as hybrid TDMA-NOMA, has been recognized as a promising solution to support massive WSN connectivity while meeting QoS requirements [7].

On the other hand, the energy constraint problem stems from the limited lifetime of the battery in a sensor. Specifically, since the sensor is small in size, its battery capacity is limited, which, as a result, shortens the sensor's lifetime [8]. This issue restricts the large-scale deployment of WSNs in areas that are difficult to reach, i.e., conventional wired charging approaches cannot be used as a frequent charging solution. In particular, such wired approaches cannot be practically deployed, as sensors are generally located in difficult-to-reach locations, such as on top of buildings, and such approaches limit the potential capabilities of sensors [9]. However, further exploitation of conventional sources contributes to an explosive growth in CO_2 emission, which has an undesirable impact on the environment. Consequently, the utilization of simultaneous wireless power and information transfer (SWIPT) has been considered an appealing solution for charging sensors' batteries and thus prolonging their lifetime. With SWIPT, sensors utilize the received radio frequency (RF) for two functions: wireless information transfer (WIT) and wireless energy transfer (WET). Specifically, the WIT is assigned for information decoding (ID), while energy harvesting (EH) is achieved in the WET. This splitting can occur by power splitting (PS) or time splitting (TS) approaches [10]. In particular, SWIPT aligns with the WSN topology, as it enables wireless charging while ensuring the exchange of information in the WSN.

Furthermore, the intelligent reflecting surface (IRS) has recently emerged as a promising candidate for supporting the demanding requirements of B5G communication systems. In particular, the IRS consists of a set of passive-reflecting elements. In particular, such reflecting elements can be intelligently tuned through a set of controllers to coordinate the reflected signals, thus improving channel propagation between the communication terminals [11]. This improvement is achieved by steering the signal into the intended direction and/or eliminating interference. Since IRS can be installed over existing infrastructure, its potential capabilities have been investigated in emerging communication applications, such as IRS-assisted wireless power transfer, IRS-assisted UAV Communications, and IRS-assisted mobile edge computing [12]. In particular, the deployment of IRS in wireless communication systems can offer different functions, such as creating a virtual line of sight (LOS) link between a transmitter (i.e., a BS) and a user when such a link is blocked due to obstacles [11]. Such a solution can offer a potential approach to improve QoS for cell-edge users. Meanwhile, the IRS can also provide other attractive functions, such as improving the channel rank between the transmitter and the receiver [11], [12]. This becomes vital in the WSN due to the potential blockages between the BS and the sensors, which are generally located in critical areas. Additionally, the IRS can be implemented on the existing communication infrastructure at a low cost. Due to these beneficial functions, the IRS has recently been integrated into several communication systems, including the WSN, where such systems are referred to as IRS-assisted WSN systems.

A. LITERATURE REVIEW

Recently, several works have investigated different IRS-assisted WSN scenarios.

1) IRS-ASSISTED WSN WITHOUT NOMA

In [13], an IRS-assisted TDMA WSN has been considered, where the available transmission time is divided into two phases: downlink (DL) and uplink (UL) phases. Specifically, it has been assumed that each sensor transmits its data to an access point (AP) during the UL duration while it harvests energy in the DL phase from the power station, where TDMA is considered to support transmission in the uplink phase. Similarly, the authors in [14] have considered an IRS-assisted TDMA WSN. However, a self-empowered IRS is considered; that is, the IRS unit can harvest energy. Consequently, the DL phase is divided into two phases, where the IRS unit harvests energy in the first phase and reflects the signal to the intended sensors in the second phase. A resource allocation technique has been developed to maximize the sum throughput. Furthermore, another IRS-assisted WSN system

TABLE 1. The key difference between our work and the existing literature.

Reference	System Model	Key Differences
[13]	IRS-assisted TDMA WPCN	NOMA transmission is not considered
[14]	IRS-assisted WPSN	NOMA transmission is not considered
[15]	IRS-aided WPCN	NOMA transmission is not considered
[16]	IoT IRS-assisted WPSN	NOMA transmission is not considered
[20]	IRS-assisted NOMA WPCN	ID is not considered in DL transmission
[21]	IRS-assisted NOMA network	Users are divided into EH and ID devices
[22]	IRS-assisted NOMA system	Cooperative NOMA is considered in Smart Agriculture
[23]	IRS-assisted IoT system	ID is not considered in DL transmission
[24]	IRS-assisted WPT	There are not ID devices
[25]	IRS-assisted WPHN	NOMA is not considered

has been proposed in [15], where the available transmission time is divided into multiple time slots; as such, the first time slot is reserved for EH by all sensors. In addition, a wireless-empowered IRS-assisted WSN has been considered in [16]. Note that NOMA transmission has not been considered in [13], [14], [15], [16].

2) IRS-ASSISTED WSN WITH NOMA

The exploitation of IRS in NOMA-based systems has been widely investigated as a potential approach for 6G networks, including the work in [17], [18], [19]. Specifically, the authors in [17] have considered the deployment of a large intelligent surface (LIS) in a NOMA downlink system, where the pairwise error probability (PEP) has been derived for NOMA users assuming imperfect successive interference cancellation. In addition, the work in [18] proposed two novel IRS systems: IRS partition-assisted and IRS quadrature NOMA systems. Furthermore, bit error rate (BER) analytical expressions have been derived for IRS-assisted power domain NOMA systems in [19]. A wireless power communication network (WPCN) has been investigated in [20]. Specifically, IRS-assisted NOMA transmission is considered, where the transmission time is split into two phases. In the first phase, sensors harvest energy while transmitting their data to the BS in the second phase. Furthermore, the IRS unit is utilized to support the DL and UL transmissions. In [21], the authors have developed an IRS-assisted WPCN NOMA-based system. In particular, the devices (i.e., the sensors) are divided into two sets: the EH and ID devices. The applications of WSN NOMA-based in smart agriculture have been demonstrated in [22]. Furthermore, an IRS-assisted wireless-powered IoT network has been discussed in [23], where the transmission time is divided into a set of sub-time slots, with each sensor allocated two slots: the EH time slot and the UL time slot. Furthermore, an IRS-Aided WPCN with NOMA has been considered in [24]. Specifically, the time frame is divided into three phases: the EH, UL transmission, and DL transmission phases. In particular, a power minimization framework has been formulated, and Federated Learning was adopted to solve the problem. On the other hand, [25] has investigated the performance of the WP heterogeneous network (WPHN), where users are classified into two sets, namely EH and non-EH devices. We summarize the key differences between the work in this paper and that in some related work in the literature in Table 1.

B. MOTIVATION AND CONTRIBUTIONS

Several configurations have been investigated for the large-scale deployment of the IRS-assisted WSN system. However, most of the existing literature has focused on deploying either TDMA or NOMA in the proposed configurations. However, the DL requirements for the WSN have not been thoroughly investigated. Consequently, this paper considers the implementation of hybrid TDMA-NOMA in IRS-assisted WSN systems. In particular, the proposed configuration effectively captures the demanding energy and information requirements of DL and UL transmissions. The main contributions of the paper are summarized as follows:

- We consider an IRS-assisted TDMA-NOMA WSN, in which sensors are grouped into clusters, and the transmission time is divided equally into two phases: the DL and UL phases. In addition, a set of IRS units is considered to assist with UL and DL transmissions.
- Specifically, the DL time is dynamically split between the clusters into sub-time slots, where each sub-time slot is reserved for each cluster to enable the sensors to perform EH and ID through a dynamic TS approach. Furthermore, it is also assumed that the UL time is divided between the clusters, so each sub-time slot is reserved for the UL transmission.

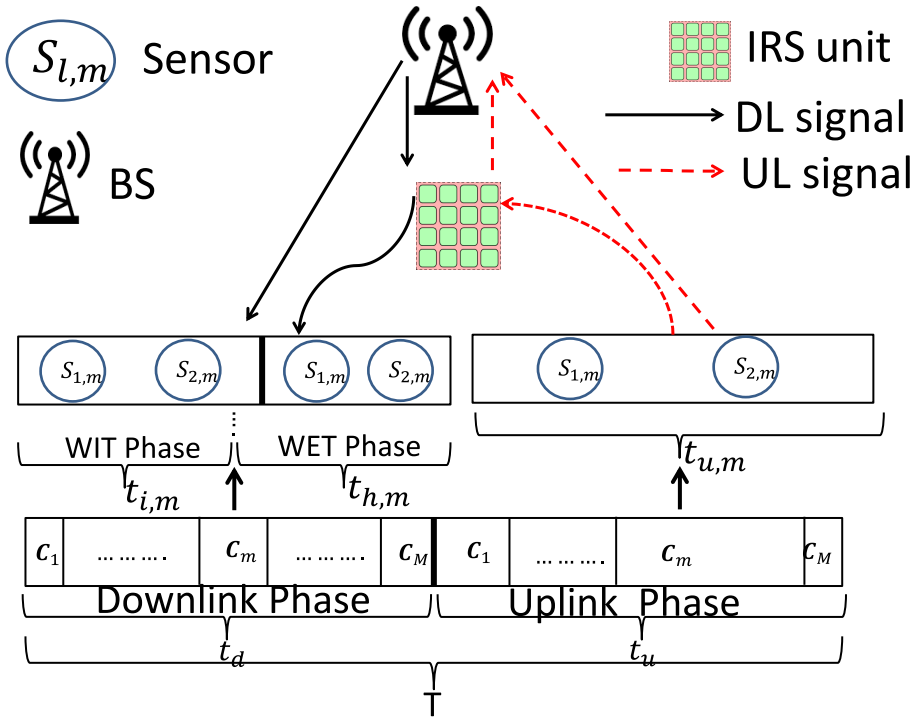

FIGURE 1. The time frame of the IRS-assisted WSN hybrid TDMA-NOMA system.

- We formulate a power minimization framework that aims to minimize the DL and UP power consumptions under a set of ID and EH requirements in the DL and UL directions. Consequently, an iterative algorithm is proposed to solve the problem and evaluate the optimization variables, i.e., the power allocated for each user and the IRS reflection coefficient matrix, in the DL and UL transmissions. To highlight the superiority of the proposed configuration, we compare its performance in simulations with two benchmark schemes.

C. PAPER ORGANIZATION

The rest of the paper is organized as follows. Section II presents the IRS-assisted WSN hybrid TDMA-NOMA configuration. The proposed power minimization framework is introduced in Section III. Then, the proposed iterative algorithm is provided in Section IV. Section V highlights the performance of the proposed configuration through a set of simulations and compares its performance against a set of benchmarks. Finally, the paper is concluded in Section VI.

II. SYSTEM MODEL

This paper considers a WSN, in which a BS communicates with K sensors. Due to size and power limitations, each communication node is equipped with a single antenna. The total transmission time is denoted as T, and is equally divided into two phases: the DL and UL phases. Specifically, the DL time slot (t_d) and the UL time slot (t_u) are reserved for DL and UL transmissions, respectively, such as $t_u = t_d = \frac{T}{2}$. In the DL and UL phases, the sensors are grouped into $M = \frac{K}{2}$ clusters, where each cluster consists of two sensors, as shown in Fig. 1. To mitigate SIC error propagation and thus facilitate NOMA transmission, sensors with diverse channel conditions are grouped. This grouping strategy has been widely adopted in NOMA-aided wireless communication systems, such as the works in [26], [27], [28], [29]. Although NOMA is capable of serving more than two users per cluster, we assume two users per cluster. This assumption facilitates the practical implementation of SIC in realistic scenarios. Furthermore, a set of M IRS units is assumed to support transmissions in the DL and UL phases. The IRS locations are assumed to be fixed in this paper, where the optimal IRS locations can be determined by incorporating the IRS locations into the optimization framework, which can be considered in our future work.

A. DOWNLINK PHASE

In the DL phase, t_d is dynamically divided into M time slots, such as $t_d = \sum_{m=1}^{M} t_{d,m}$, where $t_{d,m}$ is the allocated time slot for the m^{th} cluster ($\mathcal{C}_m$). In this phase, the BS transmits a superimposed signal to the sensors in $\mathcal{C}_m$, that is:

$$u_m = \sum_{l=1}^{2} \sqrt{p_{l,m}} u_{l,m}, \forall m \in \mathcal{M} = \{1, 2, \ldots, M\}, \quad (1)$$

where $u_{l,m}$ and $\sqrt{p_{l,m}}$ denote the symbol intended to the l^{th} sensor in the m^{th} cluster ($S_{l,m}$) and its allocated power, respectively. In particular, the sensors in each cluster employ the time-switching (i.e., TS) approach to split the received signal into two parts, the EH and ID

parts [30], [31]. Specifically, the time fraction reserved for wireless information transfer (WIT) is indicated by $t_{i,m}$, while $t_{h,m}$ is the time allocated for wireless energy transfer (WET), such as $t_{d,m} = t_{i,m} + t_{h,m}$. It is also assumed that an IRS is deployed to assist the WIT and WET in the DL phase. Accordingly, the received signal at the sensors in $\mathcal{C}_m$ can be expressed as

$$r_{l,m} = \left(h_{l,m} + \mathbf{h}_{l,m}^H \Theta_m \mathbf{g}_m\right) u_m + n_{l,m}, \forall i \in \{1, 2\}, \forall m \in \mathcal{M}, \tag{2}$$

where $\mathbf{h}_{l,m}^H \in \mathbb{C}^{1\times L}$, and $\mathbf{g}_m \in \mathbb{C}^{L\times 1}$ denote the channels between the m^{th} IRS (that is, I_m) and $S_{l,m}$, and between BS and I_m, respectively. Furthermore, $\Theta_m = \text{diag}[e^{j\theta_{m,1}}, \ldots, e^{j\theta_{m,L}}]$ is the IRS reflection diagonal matrix, where $\theta_{m,l} \in [0, 2\pi)$ is the phase shift of the l^{th} reflecting element of I_m while L represents the number of reflecting elements of I_m. In addition, $n_{l,m}$ is the additive white Gaussian noise with variance σ^2. The channel between any communicating terminals, i.e., A and B, is characterized as $\mathbf{h}_{A,B} = (\frac{1}{d_{A,B}})^{\mu}\mathbf{q}$, where μ is the path loss exponent, $d_{A,B}$ is the distance between terminals A and B, and $\mathbf{q}$ is the small-scale fading vector. Specifically, $\mathbf{q}$ is modeled as a Rayleigh fading vector following a circularly symmetric complex Gaussian distribution with zero mean and identity covariance matrix, i.e., $\mathbf{q} \sim \mathcal{CN}(0, \mathbf{I})$. Such a channel model has been widely adopted in IRS-assisted communication systems, e.g., [13], [24], [25], [32], [33].

1) THE WIT PHASE

During the WIT phase, the received signal, $t_{i,m}, \forall m$, is reserved for the identification of the sensors, where $t_{i,m}, \forall m$ represents the time allocated for the ID phase in the m^{th} cluster. Since NOMA transmission is assumed, the stronger user in each time slot should be able to decode and subtract the message of the weaker sensor before decoding its own message. Therefore, the sensors in each cluster are ordered based on their cascade channel conditions. Specifically, the first sensor in each cluster, $S_{1,m}$, is selected such that it has better channel conditions compared to the second sensor, that is,

$$\left|h_{1,m} + \mathbf{h}_{1,m}^H \Theta_m \mathbf{g}_m\right|^2 \geq \left|h_{2,m} + \mathbf{h}_{2,m}^H \Theta_m \mathbf{g}_m\right|^2. \tag{3}$$

Furthermore, similar to the existing literature, sensors with diverse channel conditions are grouped. In particular, such a clustering approach does not offer the optimal clustering strategy; however, it facilitates SIC implementation while simplifying the analysis. Consequently, the stronger sensor decodes the message of the weaker one with the following signal-to-interference and noise ratio (SINR):

$$\text{SINR}_{2,m}^{(1)} = \frac{p_{2,m}\left|h_{1,m} + \mathbf{h}_{1,m}^H \Theta_m \mathbf{g}_m\right|^2}{p_{1,m}\left|h_{1,m} + \mathbf{h}_{1,m}^H \Theta_m \mathbf{g}_m\right|^2 + \sigma^2}. \tag{4}$$

Sequentially, the stronger sensor decodes its message with the following SINR:

$$\text{SINR}_{1,m}^{(1)} = \frac{p_{1,m}\left|h_{1,m} + \mathbf{h}_{1,m}^H \Theta_m \mathbf{g}_m\right|^2}{\sigma^2}. \tag{5}$$

Unlike the stronger users, the weaker sensor directly decodes its message without SIC, with the following SINR:

$$\text{SINR}_{2,m}^{(2)} = \frac{p_{2,m}\left|h_{2,m} + \mathbf{h}_{2,m}^H \Theta_m \mathbf{g}_m\right|^2}{p_{1,m}\left|h_{2,m} + \mathbf{h}_{2,m}^H \Theta_m \mathbf{g}_m\right|^2 + \sigma^2}. \tag{6}$$

Accordingly, the achieved SINR for the sensors in each cluster can be expressed as follows:

$$\text{SINR}_{1,m} = \text{SINR}_{1,m}^{(1)}, \tag{7a}$$

$$\text{SINR}_{2,m} = \text{min.}\{\text{SINR}_{2,m}^{(1)}, \text{SINR}_{2,m}^{(2)}\}. \tag{7b}$$

With this, the achieved DL rate (i.e., rate per unit bandwidth) for each sensor can be written as follows:

$$R_{1,m}^d = t_{i,m} \log\left(1 + \text{SINR}_{1,m}\right), \tag{8a}$$

$$R_{2,m}^d = t_{i,m} \log\left(1 + \text{SINR}_{2,m}\right), \tag{8b}$$

and thus, the total downlink sum rate can be expressed as follows:

$$R^d = \sum_{m=1}^{M} \left(R_{1,m}^d + R_{2,m}^d\right) \tag{9}$$

2) THE WET PHASE

In this phase, the time fraction $t_{h,m}$ is reserved for the sensors in each cluster to harvest energy. To be specific, the harvested energy by $S_{l,m}$ can be written as:

$$E_{l,m}^h = \beta_{l,m} t_{h,m}(p_k)\left|h_{l,m} + \mathbf{h}_{l,m}^H \Theta_m \mathbf{g}_m\right|^2, \tag{10}$$

where $p_k = p_{1,m} + p_{2,m}$, while $\beta_{l,m}$ is the efficiency of the RF-DC converter. Thus, the total harvested energy can be written as follows:

$$E = \sum_{m=1}^{M} \left(E_{1,m}^h + E_{2,m}^h\right). \tag{11}$$

Note that the total transmit power at the BS is given as:

$$P^d = \sum_{m=1}^{M} \left(p_{1,m} + p_{2,m}\right). \tag{12}$$

It is worth pointing out that the phase shift of the WIT and WET phases for the m^{th} cluster, i.e., Θ_m, remains unchanged.

B. UPLINK PHASE

In the UL phase, t_u is reserved for the UL transmission from the sensors to the BS. Specifically, t_u is dynamically split into M time slots, such as $t_{u,m}$ is allocated time for $\mathcal{C}_m$, i.e., $t_u = \sum_{m=1}^{M} t_{u,m}$. In particular, NOMA is utilized for the UL

transmission from the sensors in $\mathcal{C}_m$ to the BS, where the transmit UL signal in $t_{u,m}$ can be written as:

$$y_m = \sum_{l=1}^{2} \left(v_{l,m} + \mathbf{h}_{m,\mathrm{BS}}^H \theta_m \mathfrak{h}_{\mathbf{l},\mathbf{m}} \right) \sqrt{\rho}_{l,m} \mathfrak{s}_{l,m} + n_m, \quad (13)$$

where $v_{l,m}$ is the channel between $S_{l,m}$ and the BS. Furthermore, $\mathbf{h}_{m,\mathrm{BS}}$ is the channel between the m^{th} IRS and BS, while $\mathfrak{h}_{l,m}$ represents the channel between $S_{l,m}$ and m^{th} IRS. In addition, $\mathfrak{s}_{l,m}$ and $\rho_{l,m}$ are the transmitted symbol from $S_{l,m}$ and the corresponding power level, respectively. Similar to the downlink transmission, we assume that the first sensor has better channel conditions, that is,

$$|v_{1,m} + \mathbf{h}_{m,BS}^H \theta_m \mathfrak{h}_{\mathbf{1},\mathbf{m}}|^2 \geq |v_{2,m} + \mathbf{h}_{m,BS}^H \theta_m \mathfrak{h}_{2,m}|^2. \quad (14)$$

Considering the above, the stronger sensor's message is first decoded, followed by the weaker user's message in UL transmission. Consequently, the BS decodes the message of the first sensor with the following SINR [34], [35]:

$$\mathrm{SINR}_{1,m}^u = \frac{|v_{1,m} + \mathbf{h}_{m,BS}^H \theta_m \mathfrak{h}_{1,m}|^2 \rho_{1,m}}{|v_{1,m} + \mathbf{h}_{m,BS}^H \theta_m \mathfrak{h}_{\mathbf{1},\mathbf{m}}|^2 \rho_{2,m} + \sigma^2}. \quad (15)$$

Sequentially, the BS decodes the message of the weaker sensor with the following SINR:

$$\mathrm{SINR}_{2,m}^u = \frac{|v_{2,m} + \mathbf{h}_{m,BS}^H \theta_m \mathfrak{h}_{2,m}|^2 \rho_{2,m}}{\sigma^2}. \quad (16)$$

Consequently, the achieved rates (i.e., rate per unit bandwidth) at each sensor can be expressed as [36],

$$R_{1,m}^u = t_{u,m} \log\left(1 + \mathrm{SINR}_{1,m}^u\right), \quad (17a)$$
$$R_{2,m}^u = t_{u,m} \log\left(1 + \mathrm{SINR}_{2,m}^u\right). \quad (17b)$$

The overall UL achieved sum rate can be written as:

$$R^u = \sum_{m=1}^{M} \left(R_{1,m}^u + R_{2,m}^u \right). \quad (18)$$

Furthermore, the total transmit power from the sensors in the UL can be expressed as follows:

$$P^u = \sum_{m=1}^{M} \left(\rho_{1,m} + \rho_{2,m} \right). \quad (19)$$

III. PROBLEM FORMULATION

This paper proposes a dynamic resource allocation to capture the demanding requirements of the WSN system. Specifically, the proposed resource allocation technique aims to minimize overall power consumption in the DL and UL phases, subject to achieving a set of QoS constraints. Such a power minimization framework can be formulated as follows:

$$P_1: \min_{\Lambda} \quad P = P^d + P^u \quad (20a)$$
$$\text{subject to} \quad C1: R_{l,m}^d \geq R_{\min}^d, \forall l, \forall m, \quad (20b)$$
$$C2: R_{l,m}^u \geq R_{\min}^u, \forall l, \forall m, \quad (20c)$$
$$C3: E_{l,m}^h \geq E_{l,m}^{\min}, \forall l, \forall m, \quad (20d)$$
$$C4: (3), (14), \quad (20e)$$

where $R_{\min}^u$ and $R_{\min}^d$ are the minimum DL and UL rate requirements, respectively. Furthermore, $E_{l,m}^{\min}$ denotes the minimum harvested energy requirement at each sensor, where Λ is the optimization variables set, i.e., $\Lambda = [p_{l,m}, \Theta_m, t_{i,m}, t_{h,m}, \theta_m, \rho_{l,m}, t_{u,m}]_{\forall l, \forall m}$. In particular, such a resource allocation framework captures the practical requirements of the WSN. Specifically, constraints $C1$ and $C2$ ensure that each sensor satisfies the predefined minimum DL and UL rate requirements, respectively. On the other hand, the constraint $C3$ ensures that the harvested energy by each sensor is greater than a predefined minimum threshold. Note that this minimum level can be selected to achieve sensor self-sustainability [37]. Finally, $C4$ ensures that the cascade channel gain for the first user in each cluster is greater than that for the weaker user in both the DL and UL phases.

It is clear that solving P_1 involves addressing a set of challenges. Firstly, the optimization problem P_1 is non-convex due to the non-convexity of $C1$, $C2$, $C3$, and $C4$. Secondly, the joint nature of the optimization variables introduces additional complexity when solving the problem. Next, we provide a comprehensive algorithm to solve the problem and determine the optimization variables.

IV. THE PROPOSED SOLUTION

This section provides a detailed analysis of solving the optimization problem. The DL and UL phases are independent because an orthogonal time slot is reserved for each phase. This implies that the optimization parameters for each phase can be evaluated independently of those for the other phase. In particular, we utilize the iterative algorithm, namely the sequential convex approximation (SCA), to handle the non-convexity nature of the constraints. Specifically, in SCA, each non-convex term is approximated with a linear (i.e., convex-concave) approximation using the first-order Taylor series expansion [38], [39], [40], [41], [42].

We first handle the non-convexity of $C1$ by incorporating the following set of slack variables:

$$C1: R_{l,m}^d \geq R_{\min}^d = \begin{cases} 1 + \mathrm{SINR}_{l,m} \geq \zeta_{l,m}, & (21a) \\ \zeta_{l,m} \geq 2^{z_{l,m}}, & (21b) \\ z_{l,m} \geq a_{l,m}^2, & (21c) \\ t_{i,m} a_{l,m}^2 \geq r_{l,m}, & (21d) \\ R_{l,m}^d \geq r_{l,m}, & (21e) \\ r_{l,m} \geq R_{\min}^d, & (21f) \end{cases}$$

Note that $[\zeta_{l,m}, z_{l,m}, a_{l,m}, r_{l,m}]$ is a set of slack variables. In particular, the slack variable is a non-negative variable, which is introduced as a lower bound for a non-convex term [38], [39], [40], [41], [42]. Now, we handle the non-convexity of (21a) by introducing additional slack variables. However, for the sake of notational simplicity, we assume that $|h_{l,m} + \mathbf{h}_{l,m}^H \Theta_m \mathbf{g}_m|^2 = |\mathbf{w}_{l,m}^H \Phi_m|^2$, where $\mathbf{w}_{l,m} =$

$[\mathbf{h}_{l,m}^H \text{diag}\{\mathbf{g}_m\}, \quad h_{l,m}]$ and $\Phi_m = [\Theta_m, \quad 1]$. In addition, we introduce another slack variable as follows:

$$\left|\mathbf{w}_{l,m}^H \Phi_m\right|^2 \geq \sqrt{\gamma_{l,m}}. \tag{22}$$

By incorporating the slack variables $\eta_{1,m}$, the inequality (21a) can be written as follows:

$$(21a)\begin{cases} \dfrac{p_{2,m}\sqrt{\gamma_{1,m}}}{p_{1,m}\sqrt{\gamma_{1,m}}+\sigma^2} \geq \dfrac{(\zeta_{1,m}-1)\eta_{1,m}^2}{\eta_{1,m}^2}, & (23a) \\ \dfrac{p_{1,m}\sqrt{\gamma_{1,m}}}{\sigma^2} \geq \dfrac{(\zeta_{1,m}-1)\eta_{1,m}^2}{\eta_{1,m}^2}, \forall k, & (23b) \\ \dfrac{p_{2,m}\sqrt{\gamma_{2,m}}}{p_{1,m}\sqrt{\gamma_{2,m}}+\sigma^2} \geq \dfrac{(\zeta_{2,m}-1)\eta_{2,m}^2}{\eta_{2,m}^2}. & (23c) \end{cases}$$

The constraints in (23a) can now be split into the following two constraints:

$$p_{2,m}\sqrt{\gamma_{1,m}} \geq (\zeta_{1,m}-1)\eta_{1,m}^2, \tag{24a}$$
$$\eta_{1,m}^2 \geq p_{1,m}\sqrt{\gamma_{1,m}}+\sigma^2. \tag{24b}$$

With this, the non-convexity of (24a) can now be approximated with the following two convex approximations:

$$\begin{aligned} &{p_{2,m}}^{(t)}\sqrt{\gamma_{1,m}^{(t)}}+\sqrt{\gamma_{1,m}^{(t)}}(p_{2,m}-{p_{2,m}}^{(t)}) \\ &+\frac{{p_{2,m}}^{(t)}}{2\sqrt{\gamma_{1,m}^{(t)}}}(\gamma_{1,m}-\gamma_{1,m}^{(t)}) \geq (\zeta_{1,m}^{(t)}-1){\eta_{1,m}^{(t)}}^2 \\ &+2\eta_{1,m}^{(t)}(\zeta_{1,m}^{(t)}-1)(\eta_{1,m}-\eta_{1,m}^{(t)})+{\eta_{1,m}^{(t)}}^2(\zeta_{1,m}-\zeta_{1,m}^{(t)}), \end{aligned} \tag{25}$$

where $\zeta_{1,m}^{(t)}$ is the t^{th} approximation of $\zeta_{1,m}$. Similarly, the non-convexity of (24b) can be handled as follows:

$$\begin{aligned} &{\eta_{1,m}^{(t)}}^2+2\eta_{1,m}^{(t)}(\eta_{1,m}-\eta_{1,m}^{(t)}) \geq {p_{1,m}}^{(t)}\sqrt{\gamma_{1,m}^{(t)}} \\ &+\sqrt{\gamma_{1,m}^{(t)}}(p_{1,m}-{p_{1,m}}^{(t)}) \\ &+\frac{{p_{1,m}}^{(t)}}{2\sqrt{\gamma_{1,m}^{(t)}}}(\gamma_{1,m}-\gamma_{1,m}^{(t)})+\hat{\sigma}_{1,m}^2. \end{aligned} \tag{26}$$

Note that the non-convexity of the constraints (23b) and (23c) can be handled using the same approach in (23a). Furthermore, we exploit the first-order Taylor series expansion to handle the non-convexity of (21c), (21d), and (22), which can be, respectively, written as follows:

$$z_{l,m} \geq {a_{l,m}^{(t)}}^2+2a_{l,m}^{(t)}(a_{l,m}-a_{l,m}^{(t)}), \tag{27}$$
$$t_{i,m}^{(t)}{a_{l,m}^{(t)}}^2+2t_{i,m}^{(t)}a_{l,m}^{(t)}(a_{l,m}-a_{l,m}^{(t)})+{a_{l,m}^{(t)}}^2(t_{i,m}-t_{i,m}^{(t)}) \geq r_{l,m}, \tag{28}$$

and

$$\begin{aligned} &\left|\mathbf{w}_{l,m}^H\Phi_m^{(t)}\right|^2+2\left[\Re\left(\mathbf{w}_{l,m}^H\Phi_m^{(t)}\right),\Im\left(\mathbf{w}_{l,m}^H\Phi_m^{(t)}\right)\right] \\ &\begin{bmatrix}\Re\left(\mathbf{w}_{l,m}^H\Phi_m\right)-\Re\left(\mathbf{w}_{l,m}^H\Phi_m^{(t)}\right) \\ \Im\left(\mathbf{w}_{l,m}^H\Phi_m\right)-\Im\left(\mathbf{w}_{l,m}^H\Phi_m^{(t)}\right)\end{bmatrix} \\ &\geq \sqrt{\gamma_{l,m}^{(t)}}+\frac{1}{2\sqrt{\gamma_{l,m}^{(t)}}}(\gamma_{l,m}-\gamma_{l,m}^{(t)}). \end{aligned} \tag{29}$$

Based on the above multiple relaxations, the non-convex constraint **C1** can now be replaced with the following set of convex constraints:

$$C1\text{: } r_{i,m} \geq R_{\min}^d, \text{ s. t.} \begin{cases} (21b),\ (21f),\ (23b), & (30a) \\ (23c),\ (25),\ (26), & (30b) \\ (27),\ (28),\ (29). & (30c) \end{cases}$$

We deploy SCA to handle the non-convexity of **C2.** However, for ease of notation simplicity, we let that $|v_{l,m}+\mathbf{h}_{m,BS}\theta_m\mathfrak{h}_{l,m}|^2 = |\mathbf{v}_{l,m}^H\hat{\Phi}_m|^2$, where $\mathbf{v}_{l,m} = [\mathbf{h}_{m,BS}\text{diag}\{\mathfrak{h}_{l,m}\}, \quad v_{l,m}]$ and $\hat{\Phi}_m = [\theta_m, \quad 1]$. Consequently, we introduce a set of slack variables, namely $[\zeta_{i,m}^u, z_{i,m}, \gamma_{l,m}^u, a_{i,m}^u, r_{i,m}^u]$, as follows:

$$C2\text{: } R_{i,m}^u \geq R_{\min}^u = \begin{cases} 1+\text{SINR}_{i,m}^u \geq \zeta_{i,m}^u, & (31a) \\ \zeta_{i,m}^u \geq 2^{z_{i,m}^u}, & (31b) \\ \left|\mathbf{v}_{i,m}^H\hat{\Phi}_m\right|^2 \geq \sqrt{\gamma_{l,m}^u} & (31c) \\ z_{i,m}^u \geq {a_{i,m}^u}^2, & (31d) \\ t_{u,m}{a_{i,m}^u}^2 \geq r_{i,m}^u, & (31e) \\ R_{i,m}^u \geq r_{i,m}^u, & (31f) \\ r_{i,m}^u \geq R_{\min}^u. & (31g) \end{cases}$$

Then, we deploy the same approach in **C1** to address the non-convexity of **C2**. For example, the non-convex constraint (31a) can be approximated with the following convex constraints:

$$\begin{aligned} &{\rho_{l,m}}^{(t)}\sqrt{\gamma_{l,m}^{u^{(t)}}}+\sqrt{\gamma_{l,m}^{u^{(t)}}}(\rho_{l,m}-{\rho_{l,m}}^{(t)}) \\ &+\frac{\rho_{l,m}^{(t)}}{2\sqrt{\gamma_{l,m}^{u^{(t)}}}}(\gamma_{l,m}^u-\gamma_{l,m}^{u^{(t)}}) \geq (\zeta_{l,m}^{u^{(t)}}-1){\eta_{l,m}^{u^{(t)}}}^2 \\ &+2\eta_{l,m}^{u^{(t)}}(\zeta_{l,m}^{u^{(t)}}-1)(\eta_{l,m}^u-\eta_{l,m}^{u^{(t)}})+{\eta_{l,m}^{u^{(t)}}}^2(\zeta_{l,m}^u-\zeta_{l,m}^{u^{(t)}}), \end{aligned} \tag{32}$$

$$\begin{aligned} &{\eta_{l,m}^{u^{(t)}}}^2+2\eta_{l,m}^{u^{(t)}}(\eta_{l,m}^u-\eta_{l,m}^{u^{(t)}}) \geq \rho_{o,m}^{(t)}\sqrt{\gamma_{l,m}^{u^{(t)}}} \\ &+\sqrt{\gamma_{l,m}^{u^{(t)}}}(\rho_{o,m}-{\rho_{o,m}}^{(t)}) \\ &+\frac{\rho_{o,m}^{(t)}}{2\sqrt{\gamma_{l,m}^{u^{(t)}}}}(\gamma_{1,m}^u-\gamma_{1,m}^{u^{(t)}})+\sigma^2, \forall l, o > l. \end{aligned} \tag{33}$$

Note that the constraints (31c), (31d), and (31e) are approximated with convex approximations, similar to the constraints in (29), (21c), and (21d), respectively.

THE CONSTRAINT C3

Finally, we deal with the non-convexity of **C3** by incorporating the following set of slack variables:

$$C3: E_{l,m} \geq E_{l,m}^{\min}, \text{ s. t.} \begin{cases} \left|\mathbf{w}_{l,m}^H\Phi_m\right|^2 \geq \sqrt{\gamma_{l,m}}, & (34a) \\ p_m\sqrt{\gamma_{l,m}} \geq \delta_m^2, & (34b) \\ t_{h,m}\delta_m^2 \geq e_{l,m}, & (34c) \\ \beta_{l,m}e_{l,m} \geq E_{l,m}^{\min}. & (34d) \end{cases}$$

Algorithm 1 An Iterative Algorithm to Solve the Optimization Problem P_1

Step 2: Apply SCA to approximate P_1 with P_2.
Step 3: Select a set initial variables, $\hat{\Lambda} = [\Lambda, \zeta_{l,m}, a_{l,m}, r_{l,m}, \zeta^u_{i,m}, z^u_{i,m}, a^u_{i,m}, r^u_{i,m}, \delta_m]\forall l,\forall m$.
Step 4: Repeat
1) Use CVX Package to solve P_2.
2) Update the slack variables.
Step 5: End of the Algorithm.

Note that the non-convexity of the constraint (34a) has already been handled in (29). Meanwhile, the first-order Taylor expansion can also be utilized to handle the non-convexity of (34b) and (34c). Specifically, (34b) and (34c) can be approximated with the following convex approximations:

$$p_m^{(t)}\sqrt{\gamma_{l,m}^{(t)}} + \sqrt{\gamma_{l,m}^{(t)}}\left(\gamma_{l,m} - \gamma_{l,m}^{(t)}\right) + \frac{p_m^{(t)}}{2\sqrt{\gamma_{l,m}^{(t)}}}\left(p_m - p_m^{(t)}\right) \geq {\delta_m^{(t)}}^2 + 2\delta_m^{(t)}\left(\delta_m - \delta_m^{(t)}\right), \tag{35}$$

and,

$$t_{h,m}{}^{(t)}{\delta_m^{(t)}}^2 - {\delta_m^{(t)}}^2\left(t_{h,m} - t_{h,m}{}^{(t)}\right) + 2t_{h,m}{}^{(t)}\delta_m^{(t)}\left(\delta_m - \delta_l^{(t)}\right) \geq e_{l,m}. \tag{36}$$

With the above approximations, the non-convex optimization problem P_1 can now be replaced with the following convex optimization problem:

$$P_2: \min_{\hat{\Lambda}} \; P = P^d + P^u \tag{37a}$$
$$\text{subject to } C1\text{: (21b), (23b), (23c)(25), (26), (27), (28), (29),} \tag{37b}$$
$$C2\text{: (31b), (31c), (31d), (31e), (31f), (32), (33)} \tag{37c}$$
$$C3\text{: (34d), (35), (36),} \tag{37d}$$
$$C4\text{: (3), (14).} \tag{37e}$$

Note that $\hat{\Lambda}$ is a set of optimization variables, where $\hat{\Lambda} = [\Lambda, \zeta_{l,m}, a_{l,m}, r_{l,m}, \zeta^u_{i,m}, z^u_{i,m}, a^u_{i,m}, r^u_{i,m}, \delta_m]\forall l,\forall m$. In particular, the approximated optimization problem P_2 is solved iteratively until convergence. Algorithm 1 summarizes the proposed iterative algorithm to solve the optimization problem P_1.

V. SIMULATION RESULTS

In this section, we examine the performance of the IRS-assisted WSN hybrid TDMA-NOMA with dynamic time allocation through simulations. Specifically, the proposed configuration is referred to as Dynamic IRS-assisted system throughout the simulations, and its performance is compared to two benchmarks, which are listed below.

TABLE 2. The simulation parameters.

Definition	Parameter	Value
Noise power	σ^2	-60 dBm
Number of IRS elements	L	16
Number of Sensors	K	10
Time frame	T	20 seconds
Number of IRS units	M	5
Path loss exponent	μ	3

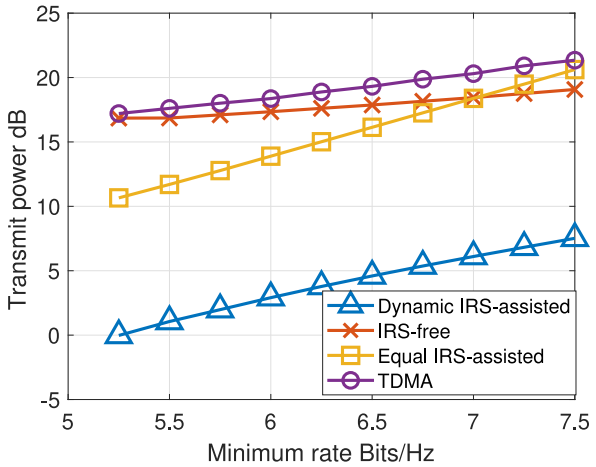

FIGURE 2. The transmit DL power, P^d, against different minimum downlink rate requirements, $E^{\min}_{l,m} = 10^{-7}$ Joule.

A. BENCHMARKS

- IRS-FREE hybrid TDMA-NOMA WSN system: In this system, it is considered that the WSN system is running without the deployment of IRS units. This system is referred to as **IRS-free system.**
- IRS-assisted hybrid TDMA-NOMA WSN system with equal time allocation: This configuration is similar to the proposed configurations. However, the DL and the UL times are equally split between the clusters. Specifically, $t_{i,m} = t_{h,m} = \frac{t_d}{2M}$, and $t_{u,m} = \frac{t_u}{M}$. This system is referred to as **Equal IRS-assisted system** throughout the simulations.

B. SIMULATION PARAMETERS

In the simulations, it is assumed that a set of 5 IRS units and 10 sensors are randomly distributed within a circle of radius 25 meters, whereas the BS is located at the center of the circle. Table 2 summarizes the simulation parameters used to generate the simulation results [43], [44], [45].

C. SIMULATION RESULTS

Fig. 2 presents the required power for DL transmission, P^d, for the proposed Dynamic IRS-assisted system and compares it with the benchmarks. The proposed dynamic IRS-assisted

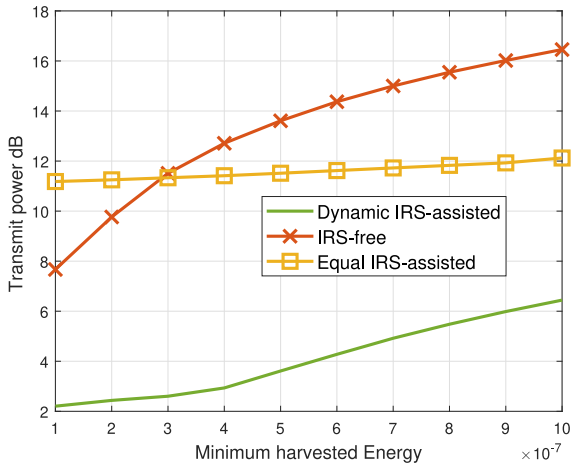

FIGURE 3. The transmit DL power, P^d, against different minimum downlink harvested energy requirements, $R^D_{\min} = 5$ (Bits/Hz).

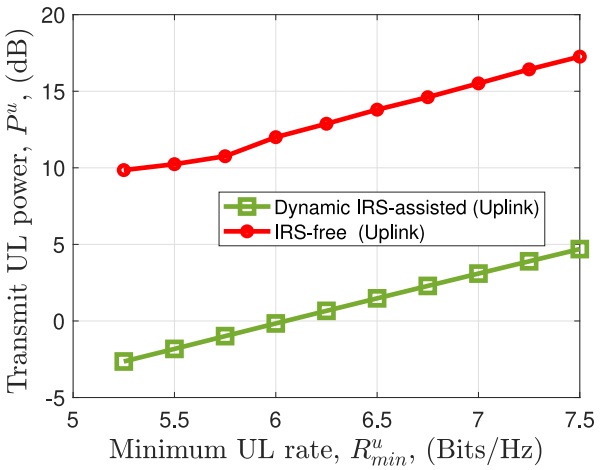

FIGURE 4. The uplink transmit power against a set of minimum uplink rate requirements.

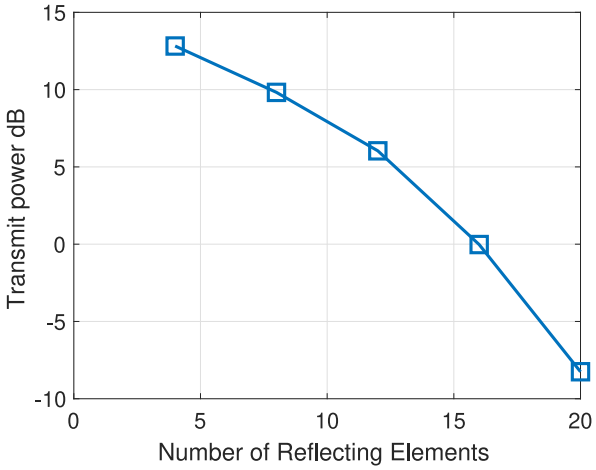

FIGURE 5. The transmit DL power, P^d, against the number of IRS elements, $E^{\min}_{l,m} = 10^{-7}$ Joule.

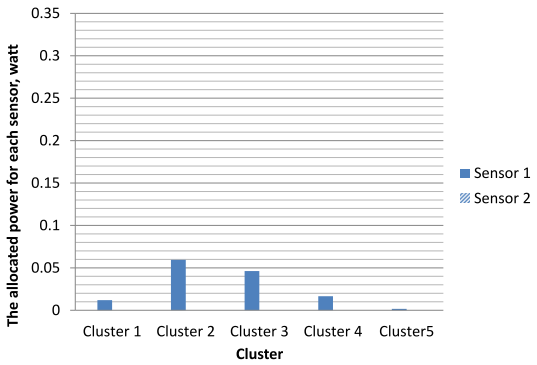

FIGURE 6. The allocated power to each sensor in the DL transmission $E^{\min}_{l,m} = 10^{-7}$ Joule.

system consumes less power to achieve minimum rate requirements compared to conventional configurations, that is, the equal IRS-assisted, TDMA, and IRS-free systems. This is because deploying the IRS units improves the cascade channel gains; thus, IRS-assisted systems consume less power than IRS-free systems. On the other hand, in the Equal IRS-assisted configuration, the time slots are allocated without considering the channel conditions of the sensors. This equal allocation policy degrades the system performance, as seen in Fig. 2. As a result, this explains the superiority of the proposed configuration compared to the benchmarks.

Fig. 3 illustrates the transmit DL power against different harvested energy requirements when $R^D_{\min} = 5$ (bits/Hz). As seen in Fig. 3, the transmit power increases with increasing minimum harvested energy requirements. However, the proposed Dynamic IRS-assisted system can achieve the QoS requirements with reduced power consumption compared to the IRS-free system. For example, the proposed Dynamic IRS-assisted system consumes one-third of the power required in the IRS-free system.

Fig. 4 sheds more light on the performance of the proposed Dynamic IRS-assisted configuration in the UL phase. Specifically, it provides the required UL transmit power, P^u, against different minimum uplink rate requirements. Since IRS units support transmission in the uplink direction, the minimum rate of uplink requirements is achieved with reduced power consumption in the IRS-assisted system compared to the IRS-free system.

Fig. 5 demonstrates the impact of varying the number of reflecting elements on the overall performance. It can be observed that increasing the number of IRS elements has a beneficial effect on power consumption.

To shed more light on the allocated power for each sensor, we have included Fig. 6, which illustrates the allocated power for each sensor. It can be seen that the sensor with a weaker channel condition in each cluster (i.e., $S_{2,m}$) is allocated a higher power level compared to the sensor with a stronger channel condition (i.e., $S_{1,m}$).

Furthermore, Fig. 7 provides the allocated time slots for each cluster in the DL phase. Specifically, Fig. 7(a) presents the allocated time for each cluster in the WIT,

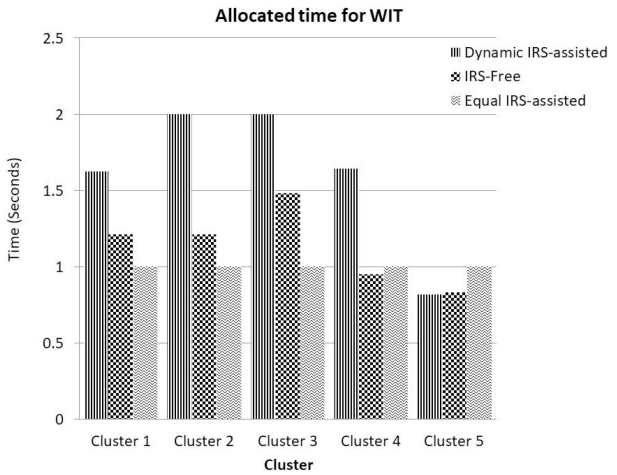

(a) Allocated time for the WIT, $t_{i,m}$

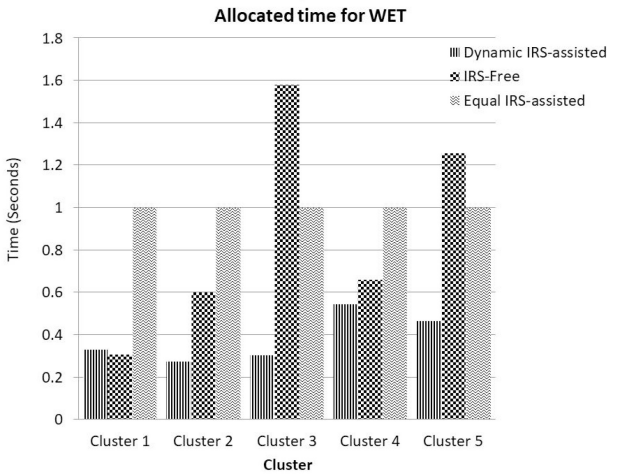

(b) Allocated time for the WET, $t_{h,m}$

FIGURE 7. Allocated time slots for the clusters in the downlink phase, $R^{d}_{\min} = 5$ Bits/Hz and $E^{\min}_{l,m} = 10^{-7}$ Joule.

whereas Fig. 7(b) shows that of the WET. Although the Equal IRS-assisted system reserves equal time slots for each cluster in the WIT and WET phases, the proposed system has dynamic time allocations. For example, the results show that Cluster one is assigned 1.36 seconds for the WIT and less than 0.3 seconds for the WET phase. Such dynamic time allocation provides additional freedom to the proposed configuration, which is reflected in the system's overall performance. In particular, since the allocated time is considered an optimization parameter, it is evaluated to minimize transmit power and capture the instantaneous channel conditions of the sensors in each cluster.

Finally, Fig. 8 illustrates the allocated time for each cluster in the UL phase for the different configurations. The proposed system offers flexible time allocation in the UL phase, considerably impacting the UL transmit power.

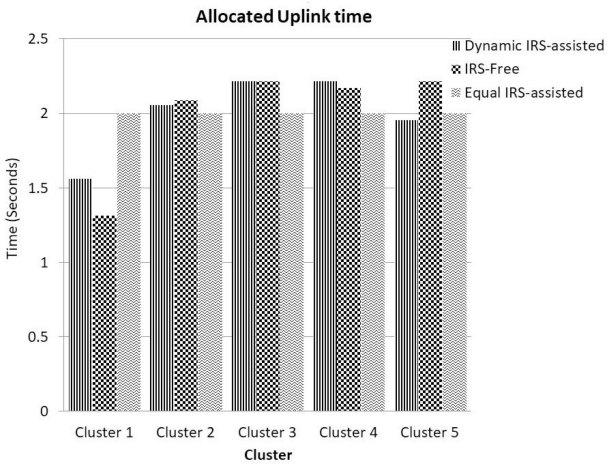

FIGURE 8. The allocated time slots for clusters in the uplink transmission.

VI. CONCLUSION

This paper investigated the IRS-assisted WSN hybrid TDMA-NOMA system. The available transmission time is divided into the DL and UL phases in this system. Consequently, the DL time is dynamically divided between the clusters for the WIT and WET phases. The sensors in each cluster decode information during the WIT phase while harvesting energy in the WET phase. However, UL transmission from the sensors to the BS is considered in the UL phase. A power minimization framework was developed to minimize the total power consumed by the system while maintaining a set of QoS constraints. Due to the non-convexity of the problem, an iterative algorithm was proposed to solve the problem. A set of simulations was presented to demonstrate the superiority of the considered configuration. Specifically, system performance was compared to two benchmarks. The simulation results confirm that the proposed dynamic configuration outperforms the conventional configurations.

REFERENCES

[1] M. Majid et al., "Applications of wireless sensor networks and Internet of Things frameworks in the industry revolution 4.0: A systematic literature review," *Sensors*, vol. 22, no. 6, p. 2087, 2022.

[2] M. N. Mowla, N. Mowla, A. S. Shah, K. M. Rabie, and T. Shongwe, "Internet of Things and wireless sensor networks for smart agriculture applications: A survey," *IEEE Access*, vol. 11, pp. 145813–145852, 2023.

[3] D. Kandris, C. Nakas, D. Vomvas, and G. Koulouras, "Applications of wireless sensor networks: An up-to-date survey," *Appl. Syst. Innov.*, vol. 3, no. 1, p. 14, 2020.

[4] F. Alawad and F. A. Kraemer, "Value of information in wireless sensor network applications and the IoT: A review," *IEEE Sensors J.*, vol. 22, no. 10, pp. 9228–9245, May 2022.

[5] D. Zhai, C. Wang, R. Zhang, H. Cao, and F. R. Yu, "Energy-saving deployment optimization and resource management for UAV-assisted wireless sensor networks with NOMA," *IEEE Trans. Veh. Technol.*, vol. 71, no. 6, pp. 6609–6623, Jun. 2022.

[6] W. Osamy, A. M. Khedr, A. Salim, A. I. Al Ali, and A. A. El-Sawy, "Coverage, deployment and localization challenges in wireless sensor networks based on artificial intelligence techniques: A review," *IEEE Access*, vol. 10, pp. 30232–30257, 2022.

[7] T. H. T. Le, Y. K. Tun, N. T. Thu, L. V. Nguyen, and E.-N. Huh, "Min-max decoding error probability optimization in RIS-aided hybrid TDMA-NOMA networks," *IEEE Access*, vol. 12, pp. 129720–129732, 2024.

[8] J. Singh, R. Kaur, and D. Singh, "Energy harvesting in wireless sensor networks: A taxonomic survey," *Int. J. Energy Res.*, vol. 45, no. 1, pp. 118–140, 2021.

[9] K. Z. Panatik et al., "Energy harvesting in wireless sensor networks: A survey," in *Proc. IEEE 3rd Int. Symp. Telecommun. Technol. (ISTT)*, 2016, pp. 53–58.

[10] T. D. P. Perera, D. N. K. Jayakody, S. K. Sharma, S. Chatzinotas, and J. Li, "Simultaneous wireless information and power transfer (SWIPT): Recent advances and future challenges," *IEEE Commun. Surveys Tuts.*, vol. 20, no. 1, pp. 264–302, 1st Quart., 2018.

[11] Q. Wu, S. Zhang, B. Zheng, C. You, and R. Zhang, "Intelligent reflecting surface-aided wireless communications: A tutorial," *IEEE Trans. Commun.*, vol. 69, no. 5, pp. 3313–3351, May 2021.

[12] S. Gong et al., "Toward smart wireless communications via intelligent reflecting surfaces: A contemporary survey," *IEEE Commun. Surveys Tuts.*, vol. 22, no. 4, pp. 2283–2314, 4th Quart., 2020.

[13] Z. Chu, Z. Zhu, F. Zhou, M. Zhang, and N. Al-Dhahir, "Intelligent reflecting surface assisted wireless powered sensor networks for Internet of Things," *IEEE Trans. Commun.*, vol. 69, no. 7, pp. 4877–4889, Jul. 2021.

[14] Z. Chu, P. Xiao, D. Mi, W. Hao, M. Khalily, and L.-L. Yang, "A novel transmission policy for intelligent reflecting surface assisted wireless powered sensor networks," *IEEE J. Sel. Topics Signal Process.*, vol. 15, no. 5, pp. 1143–1158, Aug. 2021.

[15] M. Hua, Q. Wu, and H. V. Poor, "Power-efficient passive beamforming and resource allocation for IRS-aided WPCNs," *IEEE Trans. Commun.*, vol. 70, no. 5, pp. 3250–3265, May 2022.

[16] Z. Chu et al., "Wireless-powered intelligent radio environment with nonlinear energy harvesting," *IEEE Internet Things J.*, vol. 9, no. 18, pp. 18130–18141, Sep. 2022.

[17] L. Bariah, S. Muhaidat, P. C. Sofotasios, F. El Bouanani, O. A. Dobre, and W. Hamouda, "Large intelligent surface-assisted nonorthogonal multiple access for 6G networks: Performance analysis," *IEEE Internet Things J.*, vol. 8, no. 7, pp. 5129–5140, Apr. 2021.

[18] A. Chauhan, S. Ghosh, and A. Jaiswal, "RIS partition-assisted non-orthogonal multiple access (NOMA) and quadrature-NOMA with imperfect SIC," *IEEE Trans. Wireless Commun.*, vol. 22, no. 7, pp. 4371–4386, Jul. 2023.

[19] V. C. Thirumavalavan and T. S. Jayaraman, "BER analysis of reconfigurable intelligent surface assisted downlink power domain noma system," in *Proc. Int. Conf. Commun. Syst. Netw. (COMSNETS)*, 2020, pp. 519–522.

[20] X. Li, Z. Xie, Z. Chu, V. G. Menon, S. Mumtaz, and J. Zhang, "Exploiting benefits of IRS in wireless powered NOMA networks," *IEEE Trans. Green Commun. Netw.*, vol. 6, no. 1, pp. 175–186, Mar. 2022.

[21] B. Lyu, P. Ramezani, D. T. Hoang, and A. Jamalipour, "IRS-assisted downlink and uplink NOMA in wireless powered communication networks," *IEEE Trans. Veh. Technol.*, vol. 71, no. 1, pp. 1083–1088, Jan. 2022.

[22] Z. Hu et al., "Application of non-orthogonal multiple access in wireless sensor networks for smart agriculture," *IEEE Access*, vol. 7, pp. 87582–87592, 2019.

[23] D. Kumar, C. K. Singh, O. L. A. López, V. Bhatia, and M. Latva-aho, "Performance analysis of passive/active RIS aided wireless-powered IoT network with nonlinear energy harvesting," *IEEE Trans. Wireless Commun.*, vol. 24, no. 2, pp. 1132–1145, Feb. 2025.

[24] M. Alishahi, P. Fortier, M. Zeng, Q.-V. Pham, and X. Li, "Energy minimization for IRS-aided wireless powered federated learning networks with NOMA," *IEEE Internet Things J.*, vol. 11, no. 9, pp. 16339–16350, May 2024.

[25] Z. Zhu et al., "Intelligent reflecting surface-assisted wireless powered heterogeneous networks," *IEEE Trans. Wireless Commun.*, vol. 22, no. 12, pp. 9881–9892, Dec. 2023.

[26] J. Kim, J. Koh, J. Kang, K. Lee, and J. Kang, "Design of user clustering and precoding for downlink non-orthogonal multiple access (NOMA)," in *Proc. IEEE Mil. Commun. Conf. (MILCOM)*, 2015, pp. 1170–1175.

[27] B. Kimy et al., "Non-orthogonal multiple access in a downlink multiuser beamforming system," in *Proc. IEEE Mil. Commun. Conf. (MILCOM)*, 2013, pp. 1278–1283.

[28] S. Ali, E. Hossain, and D. I. Kim, "Non-orthogonal multiple access (NOMA) for downlink multiuser MIMO systems: User clustering, beamforming, and power allocation," *IEEE Access*, vol. 5, pp. 565–577, 2017.

[29] X. Wei et al., "Resource allocation technique for hybrid TDMA-NOMA system with opportunistic time assignment," in *Proc. IEEE ICC WORKSHOP*, 2020, pp. 1–7.

[30] R. Jiang, K. Xiong, P. Fan, Y. Zhang, and Z. Zhong, "Power minimization in SWIPT networks with coexisting power-splitting and time-switching users under nonlinear EH model," *IEEE Internet Things J.*, vol. 6, no. 5, pp. 8853–8869, Oct. 2019.

[31] J. Tang et al., "Energy efficiency optimization for NOMA with SWIPT," *IEEE J. Sel. Topics Signal Process.*, vol. 13, no. 3, pp. 452–466, Jun. 2019.

[32] A. Waraiet, K. Cumanan, Z. Ding, and O. A. Dobre, "Deep reinforcement learning-based robust design for an IRS-assisted MISO-NOMA system," *IEEE Trans. Mach. Learn. Commun. Netw.*, vol. 2, pp. 424–441, Apr. 2024.

[33] J. Zhu, J. Wang, Y. Huang, S. He, X. You, and L. Yang, "On optimal power allocation for downlink non-orthogonal multiple access systems," *IEEE J. Sel. Areas Commun.*, vol. 35, no. 12, pp. 2744–2757, Dec. 2017.

[34] X. Yang, H. Wang, and Y. Feng, "Sum rate maximization for active RIS-aided uplink multi-antenna NOMA systems," *IEEE Wireless Commun. Lett.*, vol. 12, no. 7, pp. 1149–1153, Jul. 2023.

[35] M. Zeng, X. Li, G. Li, W. Hao, and O. A. Dobre, "Sum rate maximization for IRS-assisted uplink NOMA," *IEEE Commun. Lett.*, vol. 25, no. 1, pp. 234–238, Jan. 2021.

[36] M. AlaaEldin, E. Alsusa, K. G. Seddik, and M. Al-Jarrah, "Optimizing irs-assisted uplink NOMA system for power constrained IoT networks," in *Proc. IEEE 96th Veh. Technol. Conf. (VTC)*, 2022, pp. 1–6.

[37] S. Guo, Y. Shi, Y. Yang, and B. Xiao, "Energy efficiency maximization in mobile wireless energy harvesting sensor networks," *IEEE Trans. Mobile Comput.*, vol. 17, no. 7, pp. 1524–1537, Jul. 2018.

[38] L.-N. Tran, M. F. Hanif, A. Tolli, and M. Juntti, "Fast converging algorithm for weighted sum rate maximization in multicell MISO downlink," *IEEE Signal Process. Lett.*, vol. 19, no. 12, pp. 872–875, Dec. 2012.

[39] M. F. Hanif, Z. Ding, T. Ratnarajah, and G. K. Karagiannidis, "A minorization-maximization method for optimizing sum rate in the downlink of non-orthogonal multiple access systems," *IEEE Trans. Signal Process.*, vol. 64, no. 1, pp. 76–88, Jan. 2016.

[40] H. Alobiedollah, K. Cumanan, J. Thiyagalingam, A. G. Burr, Z. Ding, and O. A. Dobre, "Energy efficiency fairness beamforming designs for MISO NOMA systems," in *Proc. IEEE WCNC*, 2019, pp. 1–6.

[41] H. Al-Obiedollah, K. Cumanan, J. Thiyagalingam, A. G. Burr, Z. Ding, and O. A. Dobre, "Sum rate fairness trade-off-based resource allocation technique for MISO NOMA systems," in *Proc. IEEE WCNC*, 2019, pp. 1–6.

[42] H. Al-Obiedollah et al., "On energy harvesting of hybrid TDMA-NOMA systems," in *Proc. IEEE Globecom*, 2019, pp. 1–6.

[43] H. Wang, C. Liu, Z. Shi, Y. Fu, and R. Song, "On power minimization for IRS-aided downlink NOMA systems," *IEEE Wireless Commun. Lett.*, vol. 9, no. 11, pp. 1808–1811, Nov. 2020.

[44] J. Zuo, Y. Liu, Z. Qin, and N. Al-Dhahir, "Resource allocation in intelligent reflecting surface assisted NOMA systems," *IEEE Trans. Commun.*, vol. 68, no. 11, pp. 7170–7183, Aug. 2020.

[45] Z. Li, W. Chen, Q. Wu, K. Wang, and J. Li, "Joint beamforming design and power splitting optimization in IRS-assisted SWIPT NOMA networks," *IEEE Trans. Wireless Commun.*, vol. 21, no. 3, pp. 2019–2033, Mar. 2022.

HAITHAM AL-OBIEDOLLAH (Member, IEEE) received the B.Sc. degree from the Electrical Engineering Department, Jordan University of Science and Technology, Jordan, in 2006, and the Ph.D. degree in wireless communications from the University of York, U.K., in 2019. He is currently an Assistant Professor with the Electrical Engineering Department, The Hashemite University, Jordan. His current research interests include non-orthogonal multiple access, resource allocation techniques, beamforming designs, multi-objective optimization techniques, and convex optimization theory. He received the Kathleen Mary Stott Prize for Excellence in Research in Electronic Engineering from the University of York in 2020.

HAYTHEM BANY SALAMEH (Senior Member, IEEE) received the Ph.D. degree in electrical and computer engineering from the University of Arizona, Tucson, AZ, USA, in 2009. He is currently a Professor of communications and networking engineering with Al Ain University, Al Ain, UAE (on leave from Yarmouk University, Irbid, Jordan). He is the Dean with the Graduate Studies and Scientific Research, Al Ain University. He also holds a Visiting Professor position with Staffordshire University, Stoke-on-Trent, U.K. His research interests include wireless networking, with a focus on dynamic spectrum access, cognitive radio networking, the Internet of Things, security, and distributed protocol design. He was a recipient of the Jordan Science Research Support Foundation Prestigious Award for Distinguished Research in ICT in 2015, the Best Researcher Award for Scientific Colleges in YU in 2016, and the SRSF Award for Creativity and Technological Scientific Innovation in 2017. He has served and continues to serve on the Technical Program Committee of many international conferences.

KANAPATHIPPILLAI CUMANAN (Senior Member, IEEE) received the B.Sc. (First-Class Hons.) degree in electrical and electronic engineering from the University of Peradeniya, Sri Lanka, in 2006 and the Ph.D. degree in signal processing for wireless communications from Loughborough University, Loughborough, U.K., in 2009.

He is currently a Professor of wireless communications with the School of Physics, Engineering and Technology, University of York, U.K., where he joined as a Lecturer in November 2014. Prior to this he served as an Assistant Lecturer with the Department of Electrical and Electronic Engineering, University of Peradeniya, Sri Lanka, from January 2006 to August 2006. From January 2010 and March 2012, he held a Research Associate position with Loughborough University followed by a similar role at Newcastle University, Newcastle upon Tyne, U.K., from March 2012 to November 2014. In 2011, he was also an Academic Visitor with the Department of Electrical and Computer Engineering, National University of Singapore. He was a Research Student from Cardiff University, Wales, U.K., from September 2006 to July 2007. He has published more than 100 journal articles and conference papers which have collectively received more than 5000 Google scholar citations. His research interests include non-orthogonal multiple access, cell-free massive MIMO, physical-layer security, cognitive radio networks, convex optimization techniques, and resource allocation techniques.

Dr. Cumanan was the recipient of an overseas research student award scheme from Cardiff University.